Journal of Solid State Chemistry **164,** 51–59 (2002)
doi:10.1006/jssc.2001.9447, available online at http://www.idealibrary.com on IDEAL®

High-Temperature Synchrotron X-Ray Powder Diffraction Study of the Orthorhombic–Tetragonal Phase Transition in $La_{0.63}(Ti_{0.92},Nb_{0.08})O_3$

Roushown Ali,* Masatomo Yashima,*,[1] Masahiko Tanaka,† Hideki Yoshioka,‡ Takeharu Mori,† and Satoshi Sasaki§

*Department of Materials Science and Engineering, Interdisciplinary Graduate School of Science and Engineering, Tokyo Institute of Technology, 4259 Nagatsuta-cho, Midori-ku, Yokohama 226-8502, Japan; †Photon Factory, Institute of Materials Structure Science, High Energy Accelerator Research Organization, 1-1 Oho, Tsukuba, Ibaraki 305-0801, Japan; ‡Hyogo Prefectural Institute of Industrial Research, Suma, Kobe 654-0037, Japan; and §Materials and Structures Laboratory, Tokyo Institute of Technology, 4259 Nagatsuta-cho, Yokohama 226-8503, Japan

Received July 3, 2001; in revised form October 25, 2001; accepted November 9, 2001

The crystal structure of $La_{0.63}(Ti_{0.92},Nb_{0.08})O_3$ has been refined by the Rietveld analysis of Cu$K\alpha$ X-ray powder diffraction data collected at 23°C. This material was confirmed to have an *A*-site deficient orthorhombic perovskite-type structure with double ideal perovskite ABO_3 units along the *c*-axis (space group *Pmmm*, $Z = 2$, $a = 3.86036(5)$ Å, $b = 3.87222(5)$ Å, $c = 7.82609(9)$ Å). Lattice parameters of the same sample have been investigated *in situ* in the temperature range from 25°C to 496°C by 1.37873(3) Å synchrotron X-ray powder diffraction. The synchrotron X-ray powder diffraction technique was found to be very powerful to determine precise lattice parameters around a phase transition temperature. This compound exhibited a reversible phase transition between the orthorhombic and tetragonal phases at around 370°C. (1) The lattice parameters increased continuously with temperature, while the *b*/*a* ratio decreased continuously with temperature and became unity at the orthorhombic–tetragonal transition point. (2) No hysteresis was observed in the lattice parameter values between heating and cooling. These results of (1) and (2) suggest that the orthorhombic–tetragonal phase transition is continuous. © 2002 Elsevier Science (USA)

Key Words: **synchrotron X-ray powder diffraction; lattice parameters; phase transition; lanthanum titanate; high temperature; crystal structure; ion conductor; thermal expansion; transformation.**

1. INTRODUCTION

$La_{2/3}TiO_3$-based compounds with an *A*-site-deficient perovskite-type structure ABO_3 exhibit high ionic conductivity and dielectric constants where $A = La_{2/3+y}$, $B = (Ti_{1-x},M_x)$, and *M* is a dopant cation (1–5). This structure can be formed either by doping metal oxide such as Al_2O_3 (1, 6, 7) and Nb_2O_5 (8) into $La_{2/3}TiO_3$ or by heating $La_{2/3}TiO_{3-\delta}$ under a reducing atmosphere (4, 9–11). Several researchers studied the crystal structures of $La_{2/3}TiO_{3-\delta}$ (10,11) and $La_{(2+x)/3}(Ti_{1-x},Al_x)O_3$ (1, 12–14). The $La_{0.68}(Ti_{0.95},Al_{0.05})O_3$ exhibits a structural phase transition between low-temperature orthorhombic (*Pmmm*) and high-temperature tetragonal (*P*4/*mmm*) phases between 200°C and 400°C (12, 13). Because Nb^{5+} has a larger valence than Ti^{4+} and Al^{3+}, possibly leading to larger concentration of vacancies at the La site, it is interesting to investigate its influence on the crystal structure and the phase transition. However, the crystal structure and the phase transition of $La_{(2-x)/3}(Ti_{1-x},Nb_x)O_3$ have not been reported yet.

Doped $La_{2/3}TiO_3$ compounds have high ion conductivity (1, 8), which makes them useful as a component in solid oxide fuel cells (SOFCs). Thermal expansion and temperature dependence of lattice parameters are important factors in designing the components of the SOFCs (12, 15, 16). To determine precisely the lattice parameters, synchrotron X-ray powder diffraction is a very useful technique (17–20). We have studied the orthorhombic–tetragonal phase transition of the $La_{0.68}(Ti_{0.95},Al_{0.05})O_3$ compound by using conventional laboratory-based X-ray diffractometers (12, 13), but it was difficult to determine precise lattice parameters around the transition point. The conventional X-ray diffractometer usually has double wavelengths of $K\alpha_1 + K\alpha_2$, and produces broad diffraction peaks with asymmetric shape, leading to a complicated peak profile. In contrast, synchrotron X-ray diffraction does not have such double peaks as $K\alpha_1 + K\alpha_2$ for one reflection, but only a single peak appears. Furthermore, the synchrotron X-ray diffraction peak can be much narrower and has a relatively symmetric peak shape. As will be described later, $La_{0.63}(Ti_{0.92},Nb_{0.08})O_3$ is orthorhombic under ambient conditions and there is a very small difference between

[1]To whom correspondence should be addressed. E-mail: yashima@materia.titech.ac.jp. Fax: + 81-45-924-5630.

0022-4596/02 $35.00

the lattice parameters a and b around the orthorhombic–tetragonal phase transition temperature. Therefore, the separation between 020 and 200 peaks would be almost impossible using the conventional X-ray diffractometer.

The purpose of this study is to refine the crystal structure of $La_{0.63}(Ti_{0.92},Nb_{0.08})O_3$ by Rietveld analysis of Cu$K\alpha$ X-ray powder diffraction data collected at 23°C. The other purpose is to determine precisely the lattice parameters of this compound as a function of temperature by using the synchrotron X-ray powder diffraction technique having much higher angular 2θ resolution compared with the conventional X-ray diffraction method. In this study, we have chosen the Nb composition $x = 0.10$ in the starting powder mixture, because this starting composition had the highest purity of the perovskite phase in the samples of $La_{(2-x)/3}(Ti_{1-x},Nb_x)O_3$ ($x = 0.0$ to 0.50) (8).

2. EXPERIMENTAL PROCEDURE

2.1. Sample Preparation of the $La_{0.63}(Ti_{0.92},Nb_{0.08})O_3$ Perovskite

The compound $La_{0.63}(Ti_{0.92},Nb_{0.08})O_3$ was prepared by solid-state reactions. Starting materials were high-purity powders of La_2O_3, TiO_2 and Nb_2O_5 ($> 99.9\%$). Each material was fired separately at 1000°C for 4 hours. Fired powders were weighted by the molar ratio of La:Ti:Nb = 19:27:3. They were well mixed and ground for 1 hour as dried powders and as ethanol slurries in an agate mortar, and then the mixture was calcined in air. This process of grinding and calcination was repeated four times. The calcination temperatures/periods were 1200°C/8 hours, 1300°C/12 hours, 1300°C/12 hours, and 1350°C/12 hours, for the first, second, third and fourth processes, respectively. Powders thus obtained were ground and then pressed into pellets under a uniaxial pressure of 150 MPa. These pellets were sintered at 1350°C for 12 hours in air. The sintered material was crushed and ground to obtain the powdered sample for X-ray powder diffraction measurements.

2.2. Rietveld Refinement of the Crystal Structure at Room Temperature with Conventional X-Ray Diffraction Data

The crystal structure was refined using Cu$K\alpha$ X-ray powder diffraction data measured at 23°C. X-ray diffraction data were collected with a conventional X-ray powder diffractometer under the following experimental conditions: step scanning mode with 0.020 deg. step interval in 2θ, counting time 2 sec., Cu$K\alpha$ radiation, and 2θ range of 20–150 deg. In order to correct the zero-point shift, an internal standard silicon powder (NIST, 640b) was mixed well with the $La_{0.63}(Ti_{0.92},Nb_{0.08})O_3$ sample. To estimate accurately the lattice parameters of the $La_{0.63}(Ti_{0.92},Nb_{0.08})O_3$ sample, Rietveld analysis was carried out for the (sample + Si) mixture by using a computer program *RIETAN*-2000 (21) where the lattice parameter of the silicon standard was fixed ($a = 5.43094$ Å). The lattice parameters thus obtained were used in the Rietveld analysis for the $La_{0.63}(Ti_{0.92},Nb_{0.08})O_3$ sample without Si powder to refine the structural parameters.

2.3. High-Temperature Synchrotron X-Ray Powder Diffraction Study

2.3.1. *Equipment for high-temperature synchrotron X-ray powder diffraction.* To determine precisely the temperature dependence of lattice parameters, synchrotron X-ray powder diffraction experiments were conducted on beam line BL-3A at Photon Factory, High Energy Accelerator Research Organization (KEK), Tsukuba, Japan. Figure 1 shows a schematic layout of the beam line and the experimental setup. The beam line BL-3A consists of a bending magnet (BM2), three slits (S1, S2, and S3), and a Si(111) double-crystal monochromator (22). We sagittally focused the beam by using the second Si(111) crystal of the double-crystal monochromator. We used the triple-axis/four-circle diffractometer at the BL-3A (23) as a powder diffractometer. The size of the S4 slit for incidence beam was about 0.6×8 mm and the size of the S5 slit was 0.6×8 mm.

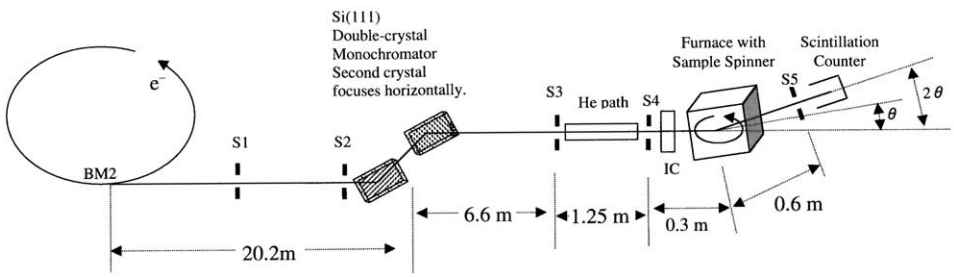

FIG. 1. Schematic layout of the beam line BL-3A and of experimental setup. e^-, BM2, S, and IC denote electron, bending magnet, slit, and ion chamber, respectively.

A small furnace (24) with Fe–Cr heaters was attached to a goniometer of the triple-axis/four-circle diffractometer, and used for synchrotron X-ray diffraction measurements at high temperatures. The sample holder was mounted in the furnace and kept rotating (1 rotation/sec) around the vertical axis of the holder plate during the X-ray diffraction measurements. This rotation technique was quite effective to obtain quality diffraction profiles and to prevent preferred orientation effects. The sample temperature was estimated using a thermocouple (Pt/Pt–13% Rh). Temperature calibration was done to obtain the relationship between the sample and the thermocouple temperatures after measuring all the high-temperature synchrotron X-ray diffraction data. Another thin thermocouple was placed just touching the sample powders to measure the sample temperature. Temperatures of the two thermocouples were recorded after waiting for 5 min. at a constant temperature. The sample temperature was kept constant within ± 1°C during each data collection.

2.3.2. *Wavelength determination.* The wavelength was determined to be $\lambda = 1.37873(3)$ Å by the calibration method described below. The profiles of eight reflections of standard reference material NBS 674 CeO_2 ($a = 5.41129(8)$ Å) were obtained by step-scanned technique and the exact peak positions $2\theta_{obs}$ were calculated using an individual profile-fitting program, *PRO-FIT* (25). The peak positions $2\theta_{obs}$ were plotted against d-spacing values determined from the lattice parameter ($a = 5.41129(8)$ Å). The wavelength λ and zero-point shift $\Delta\theta$ were then estimated using Bragg's equation,

$$\lambda = 2d \sin(\theta_{obs} + \Delta\theta),$$

through a least-squares method.

2.3.3. *High-temperature synchrotron X-ray diffraction measurements.* We measured the peak profile around the 004, 020, and 200 reflections of the orthorhombic phase, because these reflection peaks are most important to determine the lattice parameters near the transition point (12). To obtain as much many data as possible with different temperatures, we investigated only these peaks in the limited machine time. The symmetric θ–2θ scan technique was used for data collection (Fig. 1). Scanning parameters were as follows: step interval = 0.010 deg., counting time 4 s, diffraction angle 2θ range from 40.35 to 41.95 deg., temperature range 25°C–496°C. The computer program *PRO-FIT* (25) was used to estimate the exact 2θ position for each peak. The peaks were fitted with a Pearson VII type function. We have calibrated the observed diffraction angle values $2\theta_{obs}$ of the synchrotron X-ray powder diffraction data by using a zero-point shift ΔT. The ΔT value was determined by using the synchrotron X-ray peak positions measured at room temperature and the lattice parameters obtained from the Rietveld analysis (Table 1). The zero-point shift value was assumed to be independent of temperature, because the parallel-beam geometry has very little affect of the change in sample displacement and roughness on the diffraction peak positions, in contrast to the conventional Bragg–Brentano geometry (26). The lattice parameters were calculated after calibrating the synchrotron X-ray peak position value $2\theta_{obs}$ as $(2\theta_{obs} - \Delta T)$.

TABLE 1

Lattice Parameters, Structural Parameters, and Reliability Factors for $La_{0.63}(Ti_{0.92},Nb_{0.08})O_3$ Obtained by Rietveld Refinement of Conventional X-Ray Diffraction Data Measured at 23°C

$a = 3.86036(5)$ Å, $b = 3.87222(5)$ Å, $c = 7.82609(9)$ Å

Atom	Occupancy	Site	x	y	z	B(Å^2)
La	0.984(8)	La1 (1*a*)	0.0	0.0	0.0	0.43(2)
	0.285(2)	La2 (1*c*)	0.0	0.0	0.5	0.43(2)
Ti	0.919(9)	Ti (2*t*)	0.5	0.5	0.2635(2)	0.42(3)
Nb	0.081(9)	Nb (2*t*)	0.5	0.5	0.2635(2)	0.42(3)
O	1.0	O1 (1*f*)	0.5	0.5	0.0	1.01(8)
	1.0	O2 (2*s*)	0.5	0.0	0.227(1)	1.01(8)
	1.0	O3 (2*r*)	0.0	0.5	0.244(1)	1.01(8)
	1.0	O4 (1*h*)	0.5	0.5	0.5	1.01(8)

$R_{wp} = 10.35\%$, $R_p = 7.49\%$, $R_e = 6.42\%$, $R_I = 3.22\%$, $R_F = 2.14\%$, $S = R_{wp}/R_e = 1.61$

Standard Rietveld analysis agreement index (Ref. 27).

3. RESULTS AND DISCUSSION

3.1. Rietveld Refinement of the Crystal Structure at Room Temperature with Conventional x-Ray Diffraction Data

Figure 2 shows the Rietveld pattern of conventional X-ray diffraction data measured at 23°C for $La_{0.63}(Ti_{0.92},Nb_{0.08})O_3$.

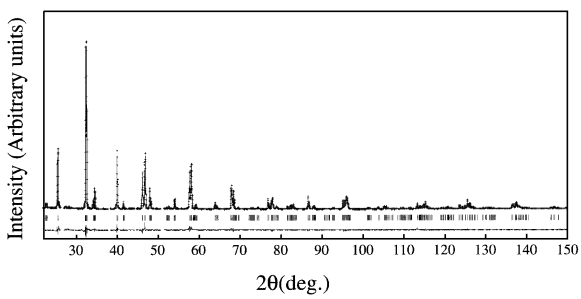

FIG. 2. Rietveld pattern of conventional X-ray diffraction data of $La_{0.63}(Ti_{0.92},Nb_{0.08})O_3$. The solid lines are calculated intensities and the crosses are observed intensities. The short vertical lines show the position of possible Bragg reflections. The difference between observed and calculated intensities is plotted below the profiles. Some 2θ regions corresponding to impurity peaks (identified as $LaNbTiO_6$ and $La_2Ti_2O_7$) were excluded from the Rietveld refinement.

TABLE 2
Selected Interatomic Distances and Bond Angles of $La_{0.63}(Ti_{0.92},Nb_{0.08})O_3$ at 23°C

Bond distance (Å)		Bond angle (deg)	
Ti,Nb–O1 × 1,	2.062(1)	O1–Ti,Nb–O2	81.5(2)
Ti,Nb–O2 × 2,	1.958(1)	O1–Ti,Nb–O3	85.4(3)
Ti,Nb–O3 × 2,	1.9365(7)	O4–Ti,Nb–O2	98.5(2)
Ti,Nb–O4 × 1	1.851(1)	O4–Ti,Nb–O3	94.6(3)
La1–O1 × 4	2.73390(4)	O1–La1–O2	58.67(8)
La1–O2 × 4	2.621(6)	O1–La1–O3	59.69(8)
La1–O3 × 4	2.717(6)	O2–La1–O3	61.67(7)
La2–O2 × 4	2.882(6)	O2–La2–O3	57.69(6)
La2–O3 × 4	2.789(7)	O2–La2–O4	61.78(7)
La2–O4 × 4	2.73390(4)	O3–La2–O4	60.55(8)

Structural refinement was successfully performed using an orthorhombic structure (space group *Pmmm*) based on the model for $La_{0.68}(Ti_{0.95},Al_{0.05})O_3$ (1, 12, 13). Table 1 shows the refined unit-cell and structural parameters and the reliability factors obtained from the Rietveld analysis. Table 2 shows the most representative bond distances and bond angles of $La_{0.63}(Ti_{0.92},Nb_{0.08})O_3$. This compound has an *A*-site-deficient perovskite-type structure with double ideal perovskite ABO_3 units along the *c*-axis as shown in Fig. 3 where $A = La_{0.63}$ and $B = (Ti_{0.92},Nb_{0.08})$. The lattice parameters of $La_{0.63}(Ti_{0.92},Nb_{0.08})O_3$ were estimated to be $a = 3.86036(5)$ Å, $b = 3.87222(5)$ Å, and $c = 7.82609(9)$ Å. The unit-cell volume of this compound $V = 116.986(2)$ Å^3 was larger than that of $La_{0.70}(Ti_{0.90},Al_{0.10})O_3$ $V = 115.886(3)$ Å^3 (28). The larger value is attributable to the larger ionic radius of the Nb^{5+} ion (0.64 Å for coordination number, $CN = 6$ (29)) than that of the Al^{3+} ion (0.535 Å for $CN = 6$ (29)). The La^{3+} ions were located at the special positions 0,0,0 and 0,0,0.5. The occupancy factors of La^{3+} at the La1 and La2 sites were refined independently and estimated to be $\sigma(La1) = 0.984(8)$ and $\sigma(La2) = 0.285(2)$, respectively. Different values between refined $\sigma(La1)$ and $\sigma(La2)$ indicate the chemical ordering of occupied La1 and defective La2 sites as shown in Fig. 3. The atomic coordinate *z* of Ti^{4+} and Nb^{5+} was refined assuming the Ti^{4+} was located at the same position 0.5,0.5,*z* as Nb^{5+}. The occupancy factors of Ti^{4+} and Nb^{5+} were refined and estimated to be $\sigma(Ti) = 0.919(9)$ and $\sigma(Nb) = 0.081(9)$, respectively, where the relation $\sigma(Ti) + \sigma(Nb) = 1$ was assumed in the Rietveld analysis. The chemical formula was determined to be $La_{0.634(5)}(Ti_{0.919(9)},Nb_{0.081(9)})O_3$ from the refined occupancy factors. Due to the formation of impurity $LaNbTiO_6$, the Nb concentration of the perovskite-type-structured compound 0.08 was smaller than the starting composition 0.10. The *z* coordinates of O2 and O3 were refined independently and estimated to be 0.227(1) and 0.244(1), respectively. These values agreed with those reported for $La_{0.70}(Ti_{0.90},Al_{0.10})O_3$ ($z(O2) = 0.23(1)$, $z(O3) = 0.24(1)$) (1), and for $La_{2/3}TiO_{2.97}$ ($z(O2) = 0.231(9)$, $z(O3) = 0.241(8)$) (11). As a result of the refinement, the Ti and Nb atoms were found to displace 0.105(2) Å from the ideal site 0.5,0.5,0.25 toward the O4 atom. In contrarst, O2 and O3 atoms displace 0.183(8) and 0.051(8) Å from the ideal sites 0.5,0,0.25 and 0,0.5,0.25, respectively, to the opposite direction along the *c*-axis. The displacement of Nb and Ti atoms made the different interatomic distances between $r(Ti,Nb–O1) = 2.062(1)$ Å and $r(Ti,Nb–O4) = 1.851(1)$ Å (Fig. 3 and Table 2). These displacements can be ascribed to the different charge between La1 and La2 sites. The La1–O1 plane has a positive charge of + 0.952, while the La2-O4 plane has a negative charge of − 1.145. Thus, the cations Ti and Nb displace toward the La2–O4 plane, while the anions O2 and O3 displace toward the La1–O1 plane. A similar displacement was observed in the $La_{0.68}(Ti_{0.95},Al_{0.05})O_3$ compound (13), where Ti and Al atoms were found to displace 0.070(8) Å from the ideal sites 0.5,0.5,0.25 toward the O4 atom. The displacement of Ti and Nb atoms by 0.105(2) Å in $La_{0.63}(Ti_{0.92},Nb_{0.08})O_3$ is larger than that of Ti and Al atoms by 0.070(8) Å in $La_{0.68}(Ti_{0.95},Al_{0.05})O_3$. This larger displacement is attributable to the larger charge of + 5 for the Nb atom than those of + 4 and + 3 for the Ti and Al atoms, respectively. Such displacements have been observed also for $La_{2/3+x}TiO_{3-\delta}$ ($x < 0.2$) (11), $La_{2/3-x}Li_{3x}TiO_3$ (30), $La_{0.33}NbO_3$ (31), and $La_{1.33-x}Li_{3x}Ti_2O_6$ (32). In the present refinement the isotropic displacement parameter of La at the La1 site *B*(La1) was assumed to be equal to *B*(La2): *B*(La) = *B*(La1) = *B*(La2). Similarly, we assumed

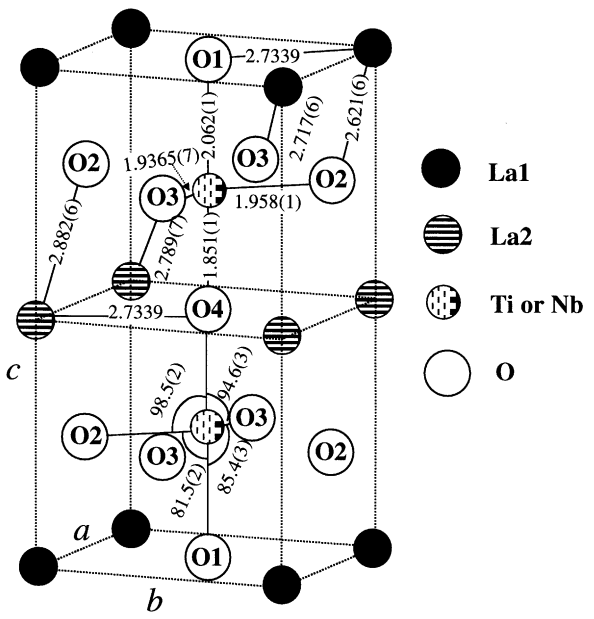

FIG. 3. Crystal structure of the $La_{0.63}(Ti_{0.92},Nb_{0.08})O_3$ compound. This picture was drawn using the present data given in Table 1.

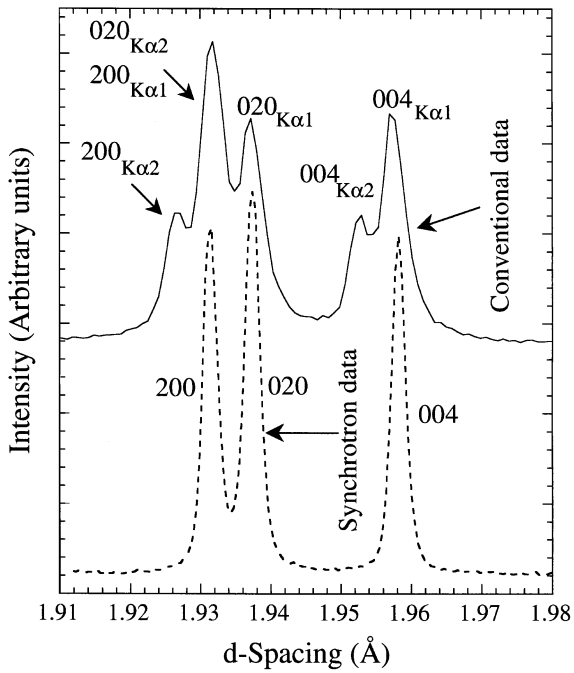

FIG. 4. Comparison between synchrotron and conventional X-ray diffraction profiles of 004, 020, and 200 reflection peaks of $La_{0.63}(Ti_{0.92},Nb_{0.08})O_3$. The lattice spacing d value on the horizontal axis was obtained from the diffraction angle 2θ by using Bragg's equation $\lambda = 2d \sin\theta$ where the values $\lambda = 1.54056$ Å and $\lambda = 1.37873$ Å were used for the conventional and synchrotron data, respectively.

B(Ti,Nb) = B(Ti) = B(Nb) and B(O) = B(O1) = B(O2) = B(O3) = B(O4). The refined B(O) value was larger than B(La) and B(Ti,Nb) as shown in Table 1.

3.2. Comparison of the High-Resolution synchrotron X-Ray Diffraction data with Conventional X-Ray Diffraction Data

Figure 4 shows a synchrotron X-ray diffraction profile around the 004, 020, and 200 reflection peaks of $La_{0.63}(Ti_{0.92},Nb_{0.08})O_3$ measured at room temperature, compared with that obtained from a conventional X-ray diffractometer. Table 3 shows the refined profile parameters both for the data measured using synchrotron X-ray radiation and for laboratory-based X-ray source. The synchrotron X-ray diffraction peaks had a narrower peak width and a more symmetric profile shape than those of the conventional X-ray diffraction ones. In fact, the full width at half-maximum W for the synchrotron source had values ranging from 0.0482 to 0.0530 (degrees in 2θ), while the conventional Cu$K\alpha$ X-ray diffraction peaks had much larger W values from 0.090 to 0.095 (Table 3). The refined asymmetry parameters A for the synchrotron diffraction profile showed values ranging from 0.97 to 1.11, while the A parameters for conventional X-ray diffraction peaks ranged from 1.65 to 2.0. Furthermore, the synchrotron X-ray did not have any doublets as $K\alpha_1$ and $K\alpha_2$ radiation peaks in the conventional X-ray source. Therefore, the synchrotron X-ray diffraction measurements enabled us to determine more

TABLE 3
Refined Parameters of the Reflection Peak Profile of $La_{0.63}(Ti_{0.92},Nb_{0.08})O_3$ Measured at Room Temperature, and Comparison of the Parameters Obtained by Synchrotron X-Ray Diffraction with those through Conventional X-Ray Diffraction

Parameters	Synchrotron radiation			Laboratory X-ray source		
hkl	004	020	200	004	020	200
Integrated intensity (counts × deg.)	4.55(5)	5.79(6)	5.12(6)	4.89(6)	4.2(1)	4.9(1)
Peak maximum position in 2θ (deg.)	40.9114(8)	41.3699(7)	41.5056(7)	46.3533(11)	46.8666(16)	47.0220(14)
FWHM in deg. W	0.0482(8)	0.0530(8)	0.0519(8)	0.091(2)	0.090(3)	0.095(3)
Asymmetry defined by $W_l/W_h A$	1.11(7)	0.97(4)	1.10(5)	1.65(8)	2.0(2)	1.9(2)
Decay rate on low-angle side R_l/η_l	2.0(2)	1.68(9)	1.68(9)	1.32(5)	1.32(5)	1.32(5)
Decay rate on high- angle side R_h/η_h	1.7(1)	2.0(1)	2.0(1)	0.90(3)	0.90(3)	0.90(3)
2θ range for fitting (deg.)		40.35–41.95			45.4–47.8	
Step width (2θ in deg.)		0.01			0.02	
Scanning time per step (sec.)		4			2	
Background parameters b_0		4.78(4)			0.89(2)	
Pattern R factor R_p		0.0323			0.0264	
Pattern weighted R factor R_{wp}		0.0428			0.0411	
Peak R factor $R_{p(peak)}$		0.0480			0.0350	
Lattice parameters (Å), a		3.86008(6)			3.8602(1)	
b		3.87207(6)			3.8723(1)	
c		7.8264(1)			7.8255(2)	

The peaks were fitted with a Pearson VII type function using individual profile fitting program *PRO–FIT* (25). All profile parameters denote the same meaning, as in Refs. (25) and (27).

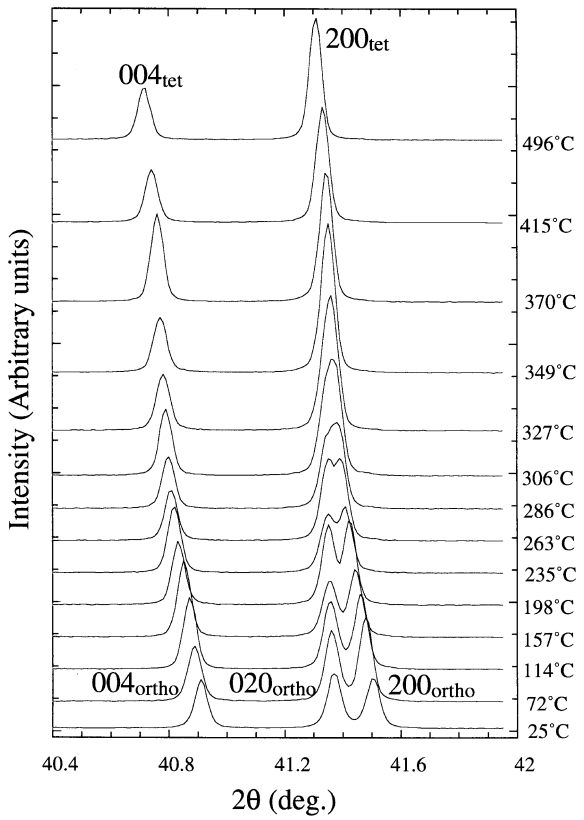

FIG. 5. Synchrotron X-ray diffraction profiles for 004, 020, and 200 reflection peaks of the $La_{0.63}(Ti_{0.92},Nb_{0.08})O_3$ compound, measured at different temperatures. Each profile was measured keeping the sample temperature constant after heating.

precisely the reflection peak positions and lattice parameters, compared with the conventional X-ray technique. The lattice parameters calculated from room temperature synchrotron X-ray diffraction data exhibited good agreement with those obtained from the Rietveld analysis (Table 1). These results demonstrate that the synchrotron X-ray diffraction is much more powerful to distinguish the 020 peak from the 200 one and to determine exactly the peak positions and lattice parameters.

3.3. Temperature Dependence of Lattice Parameters through High-Resolution Synchrotron X-Ray Diffractometry

Figure 5 shows the temperature dependence of the synchrotron X-ray diffraction profile around the 004, 020, and 200 reflection peaks during heating where each profile was measured keeping the sample temperature constant. The 004 and 200 peaks shifted to lower 2θ position with an increase of temperature due to the thermal expansion, while the 020 peak position did not change as much. Thus, at lower temperatures, the splitting between the 020 and 200 peaks was observed clearly, and the two peaks became closer to each other with increasing temperature and merged at a higher temperature. The splitting between the 020 and 200 peaks was clear up to 263°C as shown in Fig. 5. At 286°C the peak profile of the 020 and 200 reflections had a shoulder indicating the different values of 2θ positions between 020 and 200 peaks. At 306°C and 327°C we identified the sample to be also orthorhombic, because the peak widths of the 020 plus 200 reflections were significantly broader than that obtained at higher temperatures. For the data measured at 349°C and 353°C it was not easy to identify whether the sample was orthorhombic or tetragonal, so we analyzed the data assuming the orthorhombic symmetry (Table 4), while we assumed the tetragonal phase for the data measured at temperatures higher than 360°C.

TABLE 4
Lattice Parameters and Unit-Cell Volume of $La_{0.63}(Ti_{0.92},Nb_{0.08})O_3$ as a Function of Temperature

Temperature (°C)	*a* (Å)	*b* (Å)	*c* (Å)	*V* (Å^3)
Heating				
25	3.86008(6)	3.87207(6)	7.8264(1)	116.974(6)
72	3.86225(4)	3.87261(4)	7.83061(1)	117.122(5)
114	3.86382(5)	3.87313(5)	7.8335(1)	117.229(5)
157	3.86553(4)	3.87332(5)	7.8373(1)	117.343(5)
198	3.86716(4)	3.87379(4)	7.84094(9)	117.462(4)
235	3.86853(5)	3.87407(5)	7.8434(1)	117.548(5)
263	3.86968(5)	3.87411(5)	7.8454(1)	117.614(5)
286	3.87029(6)	3.87408(6)	7.8470(1)	117.656(6)
306	3.87117(5)	3.87442(5)	7.84849(9)	117.716(5)
327	3.87194(3)	3.87452(3)	7.85035(9)	117.770(3)
349	3.87307(4)	3.87460(4)	7.85227(7)	117.836(4)
370	3.87430(4)		7.85368(9)	117.885(4)
393	3.87489(4)		7.85547(9)	117.948(4)
415	3.87546(4)		7.85732(9)	118.011(4)
438	3.87610(4)		7.85894(9)	118.074(4)
461	3.87660(4)		7.85977(9)	118.117(4)
496	3.87754(4)		7.8619(1)	118.207(4)
Cooling				
57	3.86145(4)	3.87237(4)	7.8291(1)	117.069(5)
98	3.86299(4)	3.87273(4)	7.8323(1)	117.173(5)
141	3.86460(4)	3.87319(4)	7.8357(1)	117.287(5)
187	3.86641(5)	3.87353(5)	7.8384(1)	117.393(5)
205	3.86710(5)	3.87373(5)	7.8400(1)	117.444(5)
242	3.86861(4)	3.87413(4)	7.8437(1)	117.558(3)
271	3.86976(5)	3.87429(5)	7.8461(2)	117.633(6)
291	3.87032(6)	3.87415(6)	7.8467(1)	117.655(5)
312	3.87124(5)	3.87441(5)	7.8836(9)	117.716(5)
332	3.87198(4)	3.87451(4)	7.8498(1)	117.762(4)
353	3.87309(5)	3.87461(5)	7.85180(6)	117.830(4)
375	3.87425(5)		7.8536(2)	117.880(6)
397	3.87482(5)		7.8551(2)	117.939(6)
419	3.87542(4)		7.8572(2)	118.007(5)
443	3.87607(4)		7.8587(2)	118.068(5)

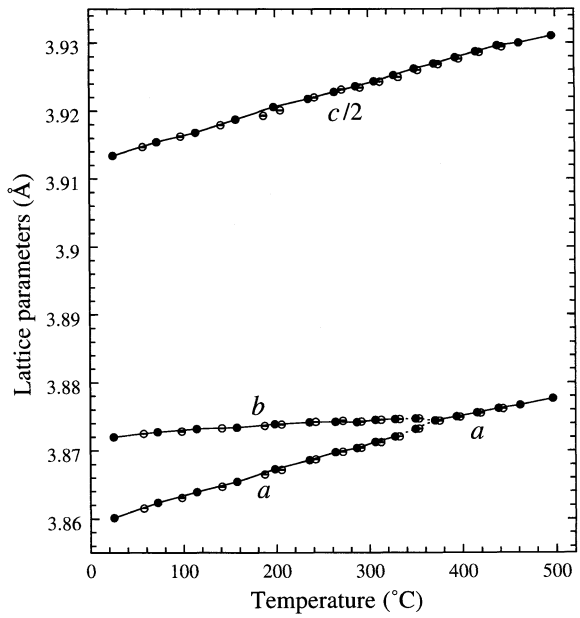

FIG. 6. Temperature dependence of the lattice parameters of the $La_{0.63}(Ti_{0.92},Nb_{0.08})O_3$ compound. Filled and open circles indicate the data obtained on heating and cooling, respectively. Dotted lines were used in the temperature region where the peak splitting between 200 and 020 reflections was not clear.

Lattice parameters obtained using the peak positions of the 004, 020, and 200 peaks are listed in Table 4 as a function of the sample temperature. Figures 6, 7, and 8 show the temperature dependence of lattice parameters, axial ratio b/a, and unit-cell volume, respectively. The lattice parameters a, b and c and the unit-cell volume increased with an increase in temperature (Figs. 6 and 8). The c/a ratio was almost independent of temperature, while the b/a decreased continuously with an increase in temperature and became unity at around 370°C (Fig. 7).

Lattice parameters obtained on heating (filled circles in Fig. 6) exhibited fairly good agreements with those on cooling (open circles in Fig. 6). Similar agreement between heating and cooling was observed also for the temperature dependence of the b/a and the unit-cell volume. Thus, (I) no hysteresis was observed in the lattice parameter values between heating and cooling (Fig. 6), and (II) the axial ratio b/a and lattice parameters changed continuously with temperature near the transition temperature (Fig. 7). The results of (I) and (II) indicate that the orthorhombic–tetragonal phase transition is continuous. It is convenient to express the temperature evolution of the order parameter of a continuous phase transition as a power law $b/a\text{-}1 = C(1 - T/T_c)^{\beta}$ at temperatures lower than T_c where the C and T_c are a coefficient independent of temperature and the transition temperature, respectively. The power exponent β is a critical exponent characterizing the temperature dependence of the order parameter. For the classical approach of mean field, $\beta = 0.5$ corresponds to a typical second-order phase transition based on Landau's phenomenology, while $\beta = 0.25$ corresponds to the tricritical phase

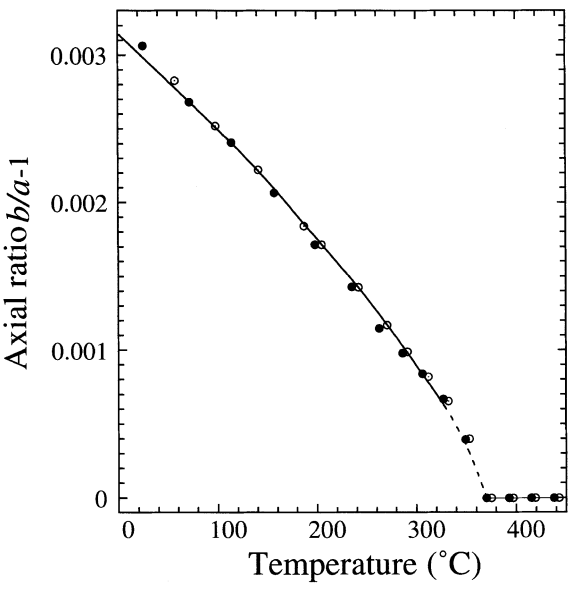

FIG. 7. Temperature dependence of the axial ratio b/a of the $La_{0.63}(Ti_{0.92},Nb_{0.08})O_3$ compound. Filled and open circles indicate the data obtained on heating and cooling, respectively. The solid line was obtained assuming a power law, $b/a - 1 = A(1 - T/T_c)^{\beta}$ where A, β, and T_c are a coefficient, critical exponent, and the transition temperature, respectively. A dashed lines was used in the temperature region where the peak splitting between 200 and 020 reflections was not clear.

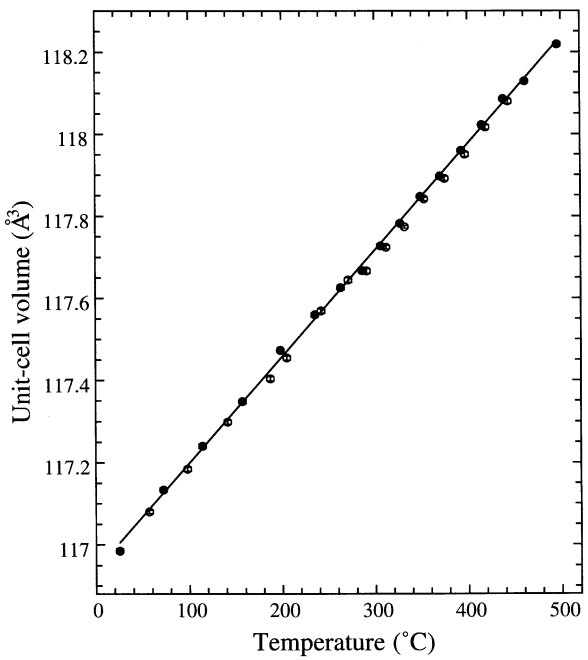

FIG. 8. Temperature dependence of the unit-cell volume of the $La_{0.63}(Ti_{0.92},Nb_{0.08})O_3$ compound. Filled and open circles indicate the data obtained on heating and cooling, respectively.

transition (33). The present data gave a higher critical exponent value $\beta = 0.74$, indicating that the order parameter $b/a - 1$ exhibits a more continuous temperature evolution, compared with that for a typical second-order phase transition based on the mean field theory.

We have demonstrated here that the axial ratio b/a of $La_{0.63}(Ti_{0.92},Nb_{0.08})O_3$ decreases continuously with increasing temperature and becomes unity at the orthorhombic–tetragonal transition temperature. Yoshioka (8) measured the ionic conductivity of the same sample and observed a continuous decrease in the activation energy with temperature. This continuous decrease of the axial ratio b/a is a possible explanation for the continuous decrease of the activation energy. A similar relationship between the ion conductivity and the lattice parameters was confirmed also for $La_{0.68}(Ti_{0.95},Al_{0.05})O_3$ (12).

We have used here a high-resolution synchrotron X-ray powder diffraction technique that has much higher angular resolution than the conventional laboratory-based X-ray diffraction. Therefore, we could determine the precise lattice parameters of the $La_{0.63}(Ti_{0.92},Nb_{0.08})O_3$ compound as a function of temperature as shown in Figs. 5 to 8. In contrast, some researchers studied the temperature dependence of lattice parameters for $La_{2/3}TiO_3$-based compounds using conventional X-ray diffraction with much lower angular resolution. We investigated the lattice parameters for the $La_{0.68}(Ti_{0.95},Al_{0.05})O_3$ compound as a function of temperature and reported that the orthorhombic structure transformed to the tetragonal phase between 192°C and 400°C (12,13). Due to the lower angular resolution, it was difficult to determine exactly the lattice parameters around the phase transition point. In this study, we were able to estimate the transition temperature more precisely, using the high-resolution synchrotron X-ray powder diffraction technique.

4. CONCLUSIONS

Rietveld refinement of Cu$K\alpha$ X-ray powder diffraction data has demonstrated that the $La_{0.63}(Ti_{0.92},Nb_{0.08})O_3$ compound has an A-site-deficient perovskite-type structure with double-ideal perovskite ABO_3 units along c-axis as shown in Fig. 3, where $A = La_{0.63}$ and $B = (Ti_{0.92},Nb_{0.08})$. Chemical ordering between La1 and La2 sites was confirmed with the occupancy factors obtained to be $\sigma(La1) = 0.984(8)$ and $\sigma(La2) = 0.285(2)$. The Ti and Nb atoms displace 0.105(2) Å from the ideal site 0.5,0.5,0.25 toward the La2–O4 plane, while O2 and O3 atoms displace 0.183(8) and 0.051(8) Å from the ideal sites 0.5,0,0.25 and 0,0.5,0.25, respectively, to the opposite direction along the c-axis.

Synchrotron X-ray powder diffraction measurements were carried out at high temperatures to investigate the precise lattice parameters as a function of temperature. Compared to the b parameter the a and c parameters increased considerably with temperature, resulting in equal a and b parameters at 370°C. With increasing temperature the b/a ratio decreased continuously and became unity at the orthorhombic–tetragonal phase transition point. Good agreements were observed in the lattice parameters and the axial ratio b/a between the data measured on heating and cooling. These results suggest that the phase transition is continuous. We found that the axial ratio b/a decreases more continuously than the order parameter of a typical second-order phase transition.

It was found that this synchrotron powder diffraction technique is very powerful to examine the temperature dependence of lattice parameters around the transition temperature, compared to conventional laboratory-based X-ray diffractometry. In the literature (17, 34–36), a number of researchers have studied the compositional dependence of lattice parameters by using high-resolution synchrotron X-ray powder diffraction at room temperature. However, there have been very few reports on the temperature dependence of lattice parameters measured *in situ* at high temperatures by using high-resolution synchrotron powder diffraction techniques, although the temperature dependence of the lattice parameters is of vital importance from the viewpoints of basic science and technology. In fact, the temperature dependence of lattice parameters directly connects with the thermal expansion, leading to important knowledge for designing of SOFC components and structural materials. Therefore, the present technique is a promising method for *in situ* characterization and the high-temperature science and technology.

ACKNOWLEDGMENTS

This study was carried out under the PAC No. 99G272, 99G046, and 2001G070. We express special thanks to Mr. S. Utsumi, H. Sugawara, K. Nakamura, Y. Fujioka, and M. Mori for experimental assistance. One of the authors (Roushown Ali) is indebted to Ministry of Education, Culture, Sports, Science and Technology of Japan (Monbu-Kagaku-sho) for the financial support provided through the Monbu-Kagaku-sho Scholarship. We express thanks also to Rigaku Co. for the conventional X-ray diffraction measurement. This work was supported partly by Grants-in-Aid for Scientific Research (B) of the Monbu-Kagaku-sho and by the Ogasawara Foundation.

REFERENCES

1. H. Yoshioka and S. Kikkawa, *J. Mater. Chem.* **8,** 1821–1826 (1998).
2. H. Yoshioka, *Jpn. J. Appl. Phys.* **33,** L945–L948 (1994).
3. J. Petzelt, E. Buixaderas, G. Komandin, A. V. Pronin, M. Valant, and D. Suvorov, *Mater. Sci. Eng. B* **57,** 40–45 (1998).
4. D. Suvorov, M. Valant, S. Skapin, and D. Kolar, *J. Mater. Sci.* **33,** 85–89 (1998).
5. M. Yokoyama, T. Ota, and I. Yamai, *J. Crystal Growth* **96,** 490–496 (1989).
6. S. Skapin, D. Kolar, and D. Suvorov, *J. Am. Ceram. Soc.* **76,** 2359–2362 (1993).

7. D. Suvorov and D. Kolar, *Ferroelectrics* **154,** 253–258 (1994).
8. H. Yoshioka, private communication, 2001.
9. J. B. Mac Chesney and H. A. Sauer, *J. Am. Ceram. Soc.* **45,** 416–422 (1962).
10. M. Abe and K. Uchino, *Mater. Res. Bull.* **9,** 147–156 (1974).
11. I.-S. Kim, T. Nakamura, Y. Inaguma, and M. Itoh, *J. Solid State Chem.* **113,** 281–288 (1994).
12. M. Yashima, R. Ali, and H. Yoshioka, *Solid State Ionics* **128,** 105–110 (2000).
13. R. Ali, M. Yashima, M. Yoshimura and H. Yoshioka, *J. Am. Ceram. Soc.* **84,** 468–470 (2001).
14. P. R. Slater and J. T. S. Irvine, *J. Solid State Chem.* **146,** 737–738 (1999).
15. N. Q. Minh, *J. Am. Ceram. Soc.* **76,** 563–588 (1993).
16. D. Skarmoutsos, A. Tsoga, A. Naoumidis, and P. Nikolopoulos, *Solid State Ionics* **135,** 439–444 (2000).
17. A. Saitow, A. Yoshikawa, H. Horiuchi, T. Shishido, T. Fukuda, M. Tanaka, T. Mori, and S. Sasaki, *J. Appl. Crystallogr.* **31,** 663–671 (1998).
18. H. Toraya, H. Hibino, and K. Ohsumi, *J. Synchrotron Rad.* **3,** 75–83 (1996).
19. M. Hart, R. J. Cernik, W. Parrish, and H. Toraya, *J. Appl. Crystallogr.* **23,** 286–291 (1990).
20. D. E. Cox, *in* "Synchrotron Radiation Crystallography" (P. Coppens, Ed.), p. 186. T. J. Press, Great Britain, 1992.
21. F. Izumi and T. Ikeda, *Mater. Sci. Forum* **321–324,** 198–204 (2000).
22. S. Sasaki, T. Mori, A. Mikuni, and H. Iwasaki, *Rev. Sci. Instrum.* **63,** 1047–1050 (1992).
23. K. Kawasaki, Y. Takagi, K. Nose, H. Morikawa, S. Yamazaki, T. Kikuchi, and S. Sasaki, *Rev. Sci. Instrum.* **63,** 1023–1026 (1992).
24. M. Tanaka, *in* "KEK Progress Report 2000-1" (Y. Murakami *et al.*, Eds.), p. 42. High Energy Acceleration Research Organization, Tsukuba, Japan, 2000.
25. H. Toraya, *J. Appl. Crystallogr.* **19,** 440–447 (1986).
26. J. B. Hastings, W. Thomlinson, and D. E. Cox, *J. Appl. Crystallogr.* **17,** 85–95 (1984).
27. R. A. Young and D. B. Wiles, *J. Appl. Crystallogr.* **15,** 430–438 (1982).
28. R. Ali, M. Yashima, H. Yoshioka, M. Tanaka, T. Mori, and S. Sasaki, *Abstracts of Annual Meeting of Crystallogr. Soc. Japan.* P3D-23, p. 108, 2000.
29. R. D. Shannon, *Acta Crystallogr. A* **32,** 751–767 (1976).
30. J. L. Fourquet, H. Duroy, and M. P. Crosnier-Lopez, *J. Solid State Chem.* **127,** 283–294 (1996).
31. V. K. Trunov, I. M. Averina, A. A. Evdokimov, and A. M. Frolov, *Sol. Phys. Crystallogr.* **26**(1), 104–105 (1981).
32. A. I. Ruiz, M. L. Lopez, M. L. Veiga, and C. Pico, *Solid State Ionics* **112,** 291–297 (1998).
33. Y. Zhao, D. J. Weidner, J. B. Parise, and D. E. Cox, *Phys. Earth Planet. Int.* **76,** 17–34 (1993).
34. M. Yashima, S. Sasaki, Y. Yamaguchi, M. Kakihana, M. Yoshimura, and T. Mori, *Appl. Phys. Lett.* **72,** 182–184 (1998).
35. H. Fujimori, M. Yashima, S. Sasaki, M. Kakihana, T. Mori, M. Tanaka, and M. Yoshimura, *Phys. Rev. B* **64,** 134104-1–5 (2001).
36. T. Hashimoto, R. Hirasawa, T. Kobayashi, H. Hirai, H. Tagawa, J. Mizusaki, H. Toraya, M. Tanaka, and K. Ohsumi, *Solid State Commun.* **102,** 561–564 (1997).